Frontiers of Information Technology & Electronic Engineering
www.jzus.zju.edu.cn; engineering.cae.cn; www.springerlink.com
ISSN 2095-9184 (print); ISSN 2095-9230 (online)
E-mail: jzus@zju.edu.cn

Supplementary materials for

Sitian WANG, Huarong ZHENG, Jianlong LI, Wen XU, 2025. Frequency of arrival-based state estimation and trajectory optimization for the navigation of autonomous marine vehicles. *Front Inform Technol Electron Eng*, 26(10):2000-2015.
https://doi.org/10.1631/FITEE.2500235

1 Sequential EKF process

The recursive solution process of the sequential EKF is as follows:

$$\hat{\boldsymbol{x}}_{\mathrm{u}}^{-}(i)=\boldsymbol{F}\hat{\boldsymbol{x}}_{\mathrm{u}}^{*}(i-1)+\boldsymbol{w}_{\mathrm{u}}, \tag{S1}$$

$$\boldsymbol{P}^{-}(i)=\boldsymbol{F}\boldsymbol{P}(i-1)\boldsymbol{F}^{\mathrm{T}}+\boldsymbol{Q}_{\mathrm{u}}, \tag{S2}$$

$$\boldsymbol{K}(i)=\boldsymbol{P}^{-}(i)\boldsymbol{H}(i)^{\mathrm{T}}\left(\boldsymbol{H}(i)\boldsymbol{P}^{-}(i)\boldsymbol{H}(i)^{\mathrm{T}}+\boldsymbol{R}_{\xi}(i)\right)^{-1}, \tag{S3}$$

$$\hat{\boldsymbol{x}}_{\mathrm{u}}^{*}(i)=\hat{\boldsymbol{x}}_{\mathrm{u}}^{-}(i)+\boldsymbol{K}(i)\boldsymbol{r}(i), \tag{S4}$$

$$\boldsymbol{P}(i)=\left(\boldsymbol{I}_{6}-\boldsymbol{K}(i)\boldsymbol{H}(i)\right)\boldsymbol{P}^{-}(i), \tag{S5}$$

where the superscript minus sign indicates a prior value, $\boldsymbol{H}(i)=\left[\nabla\boldsymbol{g}\left(\hat{\boldsymbol{x}}_{\mathrm{u}}^{-}(i)\right);\frac{\partial z_{\mathrm{u}}(i)}{\partial\hat{\boldsymbol{x}}_{\mathrm{u}}^{-}(i)^{\mathrm{T}}}\right]$, with $\nabla\boldsymbol{g}(\cdot)=\left[\frac{\partial g(i-N+1)}{\partial\cdot},...,\frac{\partial g(i)}{\partial\cdot}\right]^{\mathrm{T}}$ and $\frac{\partial z_{\mathrm{u}}(i)}{\partial\hat{\boldsymbol{x}}_{\mathrm{u}}^{-}(i)^{\mathrm{T}}}=[0,0,1,0,0,0]$.

2 Fisher information matrix for AUV state estimation

With the estimated AUV states $\hat{\boldsymbol{x}}_{\mathrm{u}}(i)$ at the i^{th} step, we can define the matrix element of the FIM, $\boldsymbol{J}$, as follows (Ramezani et al.2013):

$$\begin{aligned}\left[\boldsymbol{J}(i)\right]_{a,b}=&\nabla(i)_{a}\boldsymbol{R}_{\xi}(i)^{-1}\nabla(i)_{b}\\&+\frac{1}{2}\mathrm{tr}\left(\boldsymbol{R}_{\xi}(i)^{-1}\frac{\partial\boldsymbol{R}_{\xi}(i)}{\partial x(i)_{a}}\boldsymbol{R}_{\xi}(i)^{-1}\frac{\partial\boldsymbol{R}_{\xi}(i)}{\partial x(i)_{b}}\right),\end{aligned} \tag{S6}$$

where $\nabla(i)_{a}=\partial\left[\boldsymbol{g}\left(\hat{\boldsymbol{x}}_{\mathrm{u}}^{*}(i)\right);z_{\mathrm{u}}(i)\right]/\partial x(i)_{a}{}^{\mathrm{T}}$, $\cdot_{a,b}$ denote elements in row a, column b of the matrix, and:

$$\frac{\partial\boldsymbol{g}\left(\hat{\boldsymbol{x}}_{\mathrm{u}}^{*}(i)\right)}{\partial x(i)_{a}}=\left[\frac{\partial g(i-N+1)}{\partial x(i)_{a}},...,\frac{\partial g(i)}{\partial x(i)_{a}}\right]^{\mathrm{T}}, \tag{S7}$$

and:

$$\frac{\partial\boldsymbol{R}_{\xi}(i)}{\partial x(i)_{a}}=\mathrm{diag}\left(\frac{\partial[\boldsymbol{R}_{\xi}(i)]_{1,1}}{\partial x(i)_{a}},...,\frac{\partial[\boldsymbol{R}_{\xi}(i)]_{N,N}}{\partial x(i)_{a}}\right), \tag{S8}$$

and $x(i)_{a}$ is the a^{th} element of $\hat{\boldsymbol{x}}_{\mathrm{u}}^{*}(i)$, i.e, $\hat{\boldsymbol{x}}_{\mathrm{u}}^{*}(i)=[x(i)_{1},...,x(i)_{6}]^{\mathrm{T}}$.

For $\sigma^{2}(i)$ in Eq. (10), which is distance-dependent noise, the partial derivatives $\frac{\partial\sigma^{2}(i)}{\partial x(i)_{a}}$ for $a=1,2,...,6$ required to calculate $\frac{\partial\boldsymbol{R}_{\xi}(i)}{\partial x(i)_{a}}$ in Eq. (S8) is as follows:

$$\frac{\partial\sigma^{2}(i)}{\partial x(i)_{a}}=\frac{K_{E}}{\beta}A\left(l(i),f_{0}\right)\left(\beta+l(i)\ln L(f_{0})\right)\frac{\partial l(i)}{\partial x(i)_{a}}, \tag{S9}$$

where $l(i) = \|\hat{\boldsymbol{x}}_{\mathrm{u}}^{*}(i) - \boldsymbol{x}_{\mathrm{s}}(i)\|$.

The FIM is dependent on the relative position and relative velocity between the USV and AUV. Varying USV–AUV geometry leads to varying FIMs and thus varying observability. For measurements with stochastic noises, a higher observability of the AUV corresponds to a greater amount of information about the AUV state, which in turn leads to a higher level of estimation accuracy.

3 Optimal USV trajectory planning for AUV state estimation

The cost function ($F(k)$) is designed to optimize the USV's trajectory for accurate AUV state estimation. A key component, $F_1(k)$, is derived from the CRLB, which determines the FIM via (CRLB = FIM^{-1}). A smaller CRLB indicates better observability of the AUV state. The diagonal elements of the FIM, which dominate the CRLB, are computed from Eq. (S6) when $a = b$, and are proportional to the partial derivatives of the FOA measurements with respect to the AUV state. These partial derivatives increase with larger relative state changes between the USV and AUV, as well as with a larger Doppler. From the Doppler calculation formula, the Doppler shift is maximized when the USV velocity is opposite to the AUV velocity. Thus, when the USV moves away from the AUV, the relative state difference is maximized, leading to larger FIM diagonal elements and improved estimation accuracy. This is illustrated in Figs. S1–S4, which show the relationship between the USV's velocity direction (relative to the x-axis) and the sum of the FIM diagonal elements under varying relative positions. The figures confirm that the USV's optimal trajectory tends to be curved, moving opposite to the AUV velocity to enhance observability.

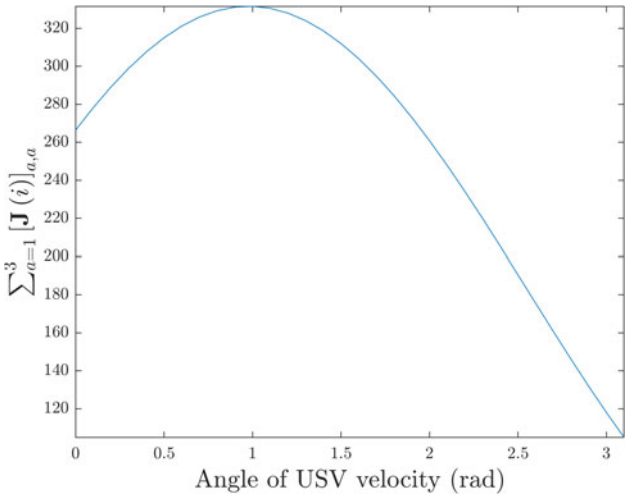

Fig. S1 Relationship between the USV's velocity direction (relative to the x-axis) and the sum of the FIM diagonal elements. AUV is positioned at $[0,0,100]^{\mathrm{T}}$ m with a velocity of $[1,0,0]^{\mathrm{T}}$ m/s, while the USV moves at a speed of 2 m/s from its position $[10,10,0]^{\mathrm{T}}$ m. The horizontal axis represents the angle between the USV velocity vector and the x-axis, and the vertical axis denotes the sum of the diagonal elements of the FIM

Similarly, when the USV moves along a straight line, the relative motion between the USV and AUV is often constrained, especially if the USV velocity aligns with the AUV velocity direction. This reduces the variability in the relative state, leading to smaller partial derivatives and a larger CRLB, which decreases observability. In contrast, a curved USV trajectory introduces greater variability in the relative position and velocity, maximizing the partial derivatives and decreasing the CRLB.

4 Parameter selection and sensitivity analysis for the cost function

The parameters α_1, α_2, and α_3 in the cost function $F(k)$ are selected to balance the contributions of $F_1(k)$, $F_2(k)$, and $F_3(k)$, based on their magnitudes. The sensitivity analysis is conducted in setting the

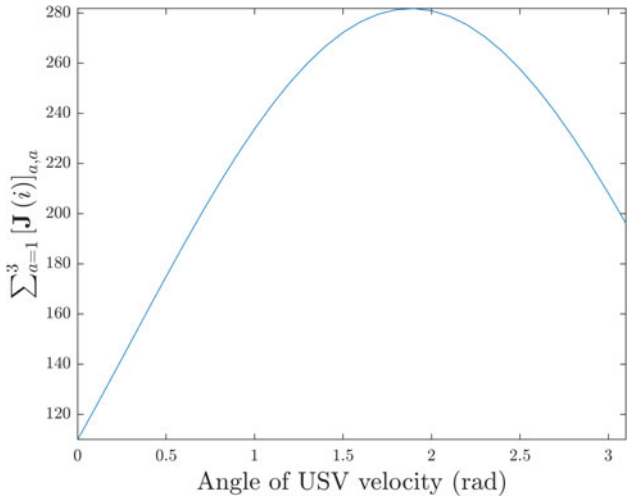

Fig. S2 **Relationship between the USV's velocity direction (relative to the x-axis) and the sum of the FIM diagonal elements. USV position is $[0, 10, 0]^{\mathbf{T}}$ m**

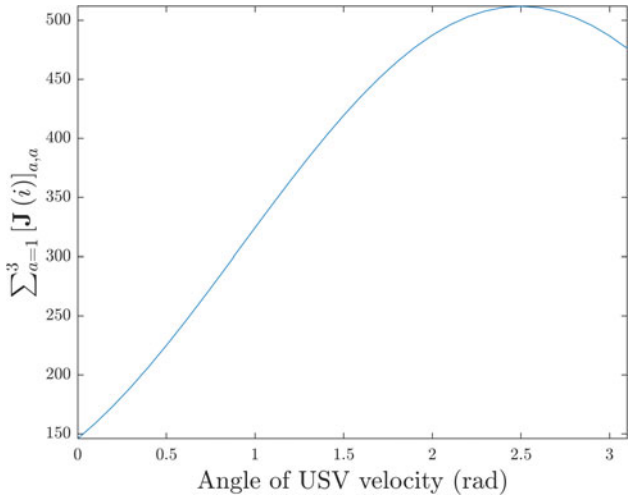

Fig. S3 **Relationship between the USV's velocity direction (relative to the x-axis) and the sum of the FIM diagonal elements. USV position is $[-10, 10, 0]^{\mathbf{T}}$ m**

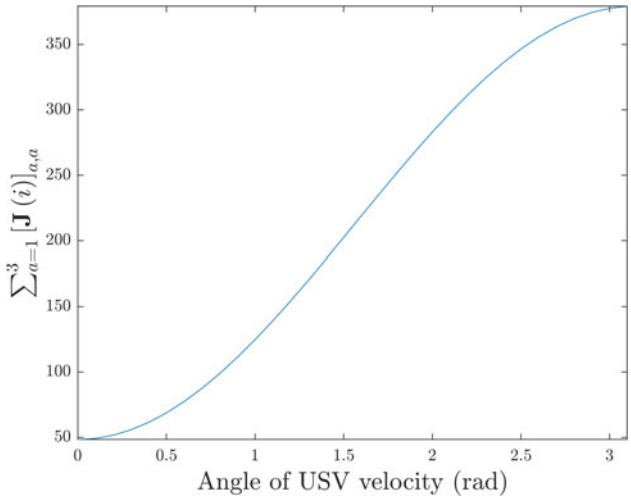

Fig. S4 **Relationship between the USV's velocity direction (relative to the x-axis) and the sum of the FIM diagonal elements. USV position is $[0, 10, 0]^{\mathbf{T}}$ m**

values of these parameters, with results summarized in Table S1. For Case 1, setting $\alpha_2 = 0.1$ yields the smallest RMSE.

Table S1 Parameter sensitivity analysis in Case 1

α_2	0.01	0.1	0.5	1	2
RMSE_x (m)	20.6	18.5	28.3	26.0	24.5
RMSE_v (m/s)	1.11	0.73	1.07	0.79	0.83

5 Simulation parameters and experimental setup

In the simulations, unless otherwise stated, the default parameters are shown in Table S2, where T denotes the total runtime of the AUV. In this scenario, the total number of steps is $I = \frac{T}{T_0} = 150$. The default noise standard deviations are shown in Table S3. The acceleration parameters for the USV and AUV ($\sigma_{\text{s,a}}$ and $\sigma_{\text{u,a}}$) are informed by their operational environments, with the USV's setting of 0.1 m/s^2 reflecting typical surface wave effects and the AUV's 0.003 m/s^2 aligning with stable underwater conditions, as supported by wave-induced motion models (Holthuijsen, 2010). The default noise standard deviations, including those for FOA measurement noise (σ), depth measurement noise (σ_z), and sound speed measurement noise (σ_{c}), are carefully selected to mirror realistic ocean conditions, with validation provided by experimental data in our prior work (Wang et al., 2025). The bounds for the USV control inputs are set as $\underline{\omega} = -\frac{\pi}{12}$ rad/s, $\bar{\omega} = \frac{\pi}{12}$ rad/s, $\bar{v} = 1.15 \left\|[v_{\text{u},x}, v_{\text{u},y}]\right\| = 2.3$ m/s, and $\underline{v} = 0.9\bar{v} = 2.07$ m/s. The initial eight steps of USV states and Doppler shifts (FOAs can be calculated as the Doppler shifts plus the center frequency of the acoustic signal) are set in Table S4. The default depth of the USV is set to 0 m, and the default velocity at depth is set to 0 m/s. The AUV's initial state is $[200\text{ m}, 200\text{ m}, 100\text{ m}, 2\text{ m/s}, 0\text{ m/s}, 0.2\text{ m/s}]^{\text{T}}$. The AUV moves along either a straight-line or curved trajectory with a slowly varying velocity. The FOA measurement noise used in the simulation is distance-dependent noise, which can be calculated using Eq. (11). The noise is concentrated around –60 Hz^2 in dB or 0.001 Hz, as shown in Table 1.

Table S2 Default parameters for the USV–AUV navigation

T (s)	N	M	P_1	f_0 (kHz)	T_0 (s)	c_0 (m/s)
450	8	3	30%	1.5	3	1500

Table S3 Default noise standard deviations

$\sigma_{\text{s,a}}$ (m/s^2)	$\sigma_{\text{u,a}}$ (m/s^2)	σ (Hz)	σ_z (m)	σ_{c} (m/s)
0.1	0.003	0.001	0.001	3

We evaluate the effectiveness of the proposed estimation framework in five cases, where the AUV follows different trajectories, as shown in Fig. S5. In Case 1, the AUV moves along a straight-line trajectory. In Cases 2–4, the AUV follows a trajectory with turning rates of $\left[\frac{\pi}{1800}, \frac{\pi}{360}, \frac{\pi}{180}\right]$ rad/s, respectively. In Case 5, the AUV trajectory is divided into five segments, each with different turning rates and/or speeds in depth: $\left[0, -\frac{\pi}{360}, \frac{\pi}{360}, -\frac{\pi}{180}, 0\right]$ rad/s and $[0.2, 0.2, 0.2, -0.2, -0.2]$ m/s.

To evaluate the optimized USV trajectory, we compare it with four specific USV trajectories, as shown in Fig. S6. Whether optimized or not, each USV trajectory is generated based on the estimated AUV state. Fig. S6 illustrates these four specific USV trajectories alongside a smooth straight-line AUV trajectory. The "LinearFollow" trajectory simply follows the AUV, while the other three sinusoidal-shaped "SinFollow" trajectories exhibit varying forms.

Table S4 Initial USV state settings for the simulation

Step No.	Position (m)		Velocity (m/s)		Doppler shift (Hz)
	x_{s}	y_{s}	$v_{\mathrm{s,x}}$	$v_{\mathrm{s,y}}$	
1	200.0	200.0	1.94	–1.23	–1.9919
2	205.8	196.3	1.79	–0.56	–4.2699
3	211.2	194.6	2.30	–0.09	–4.0335
4	218.1	194.4	2.24	0.51	–3.7841
5	224.8	195.9	2.04	1.07	–3.6143
6	231.0	199.1	2.24	0.51	–4.0156
7	237.7	200.6	2.30	–0.09	–4.0030
8	244.6	200.3	1.76	–0.55	–3.8792

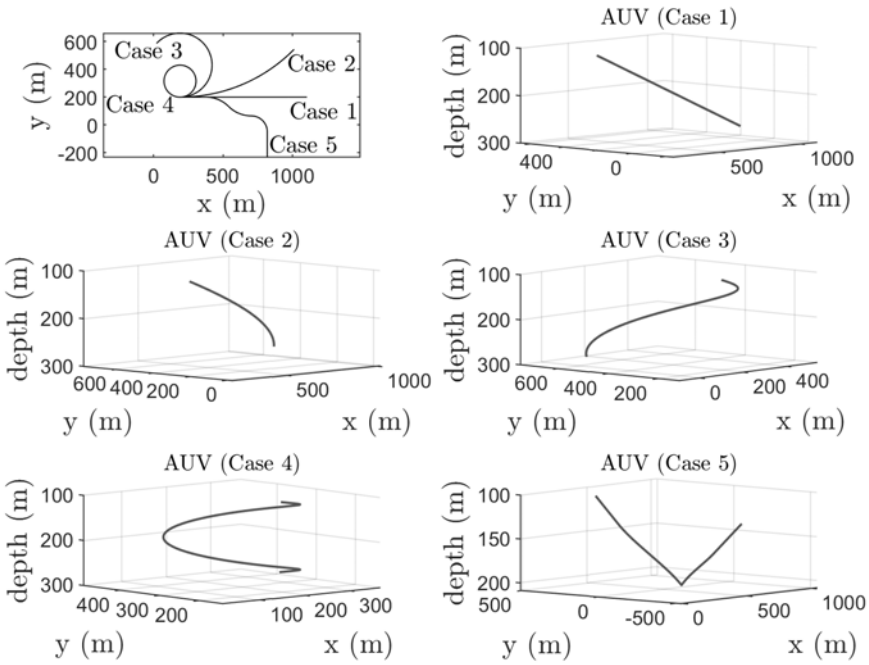

Fig. S5 AUV trajectories in Cases 1–5

The noises vary in each Monte Carlo experiment. Performance is measured using absolute errors (AE) and RMSE. Whereas RMSE shows the total estimation error over all steps, AE characterizes the estimation error at each measurement step. The AE of the i^{th} step can be obtained by $AE_i(\cdot) = |\cdot(i) - \hat{\cdot}(i)|$. By observing E times, the RMSE is calculated by:

$$\mathrm{RMSE}_x = \sqrt{\frac{1}{E}\sum_{e=1}^{E}\frac{1}{I}\sum_{i=1}^{I}\left\|\boldsymbol{x}_{\mathrm{u}}(i,e) - \hat{\boldsymbol{x}}_{\mathrm{u}}(i,e)\right\|^2}, \tag{S10}$$

$$\mathrm{RMSE}_v = \sqrt{\frac{1}{E}\sum_{e=1}^{E}\frac{1}{I}\sum_{i=1}^{I}\left\|\boldsymbol{v}_{\mathrm{u}}(i,e) - \hat{\boldsymbol{v}}_{\mathrm{u}}(i,e)\right\|^2}, \tag{S11}$$

where $\cdot(i,e)$ denotes the i^{th} step of the e^{th} Monte Carlo experiment. In the following simulations, the number of Monte Carlo experiments, E, is set to 100.

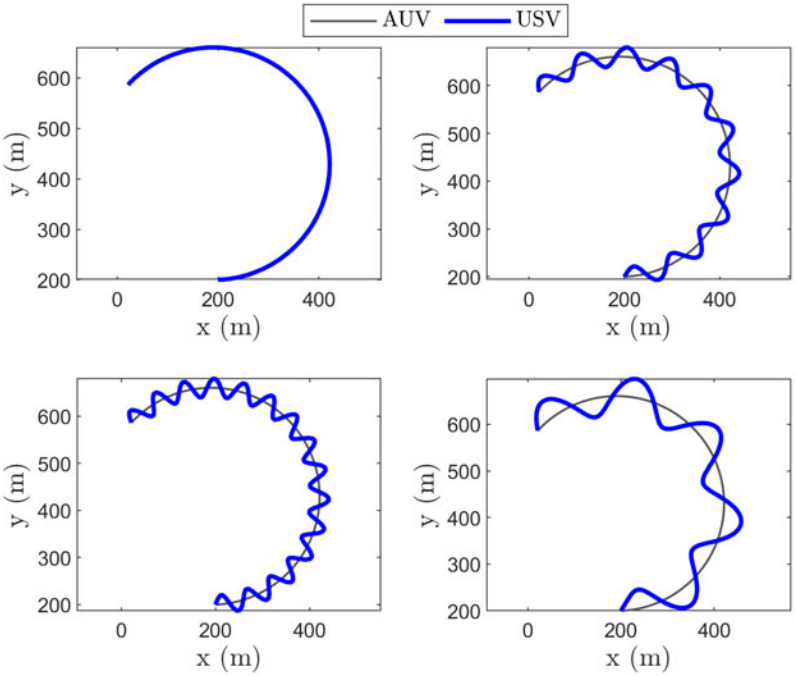

Fig. S6 Four USV specific trajectories labeled for the true AUV trajectory in Case 3. From top to bottom and left to right, as LinearFollow, SinFollow 1, SinFollow 2, and SinFollow 3, respectively

6 Comparative analysis of USV trajectory performance

Figs. S7–S9 depict the USV moving along the optimised trajectory alongside the four designated trajectories above the AUV in Cases 1, 3, and 5, respectively. Furthermore, the control inputs for the USV are illustrated in Figs. S10 and S11.

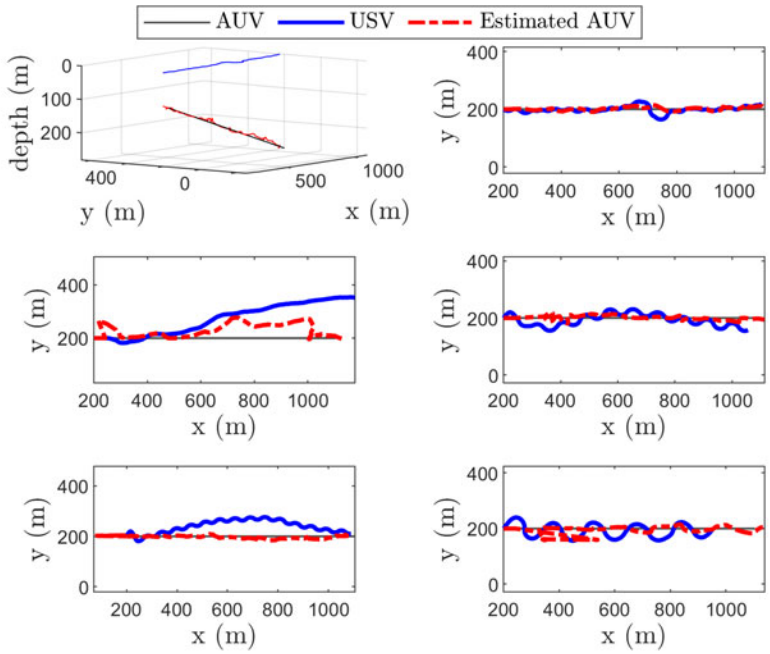

Fig. S7 USV moves along the optimized trajectory and the four specific trajectories in Case 1. The thin black line represents the AUV, the thick blue line represents the USV, and the dashed red line represents the estimated AUV trajectory. The first subfigure shows the 3D trajectories for the optimized USV. The remaining five subfigures, arranged from left to right and top to bottom, display the 2D optimized, LinearFollow, SinFollow 1, SinFollow 2, and SinFollow 3 trajectories, respectively

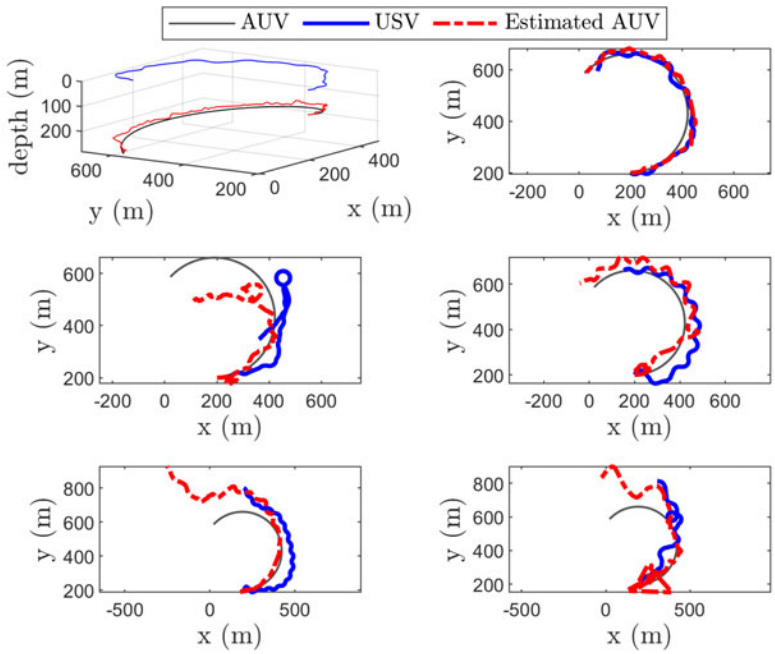

Fig. S8 USV moves along the optimized trajectory and the four specific trajectories in Case 3

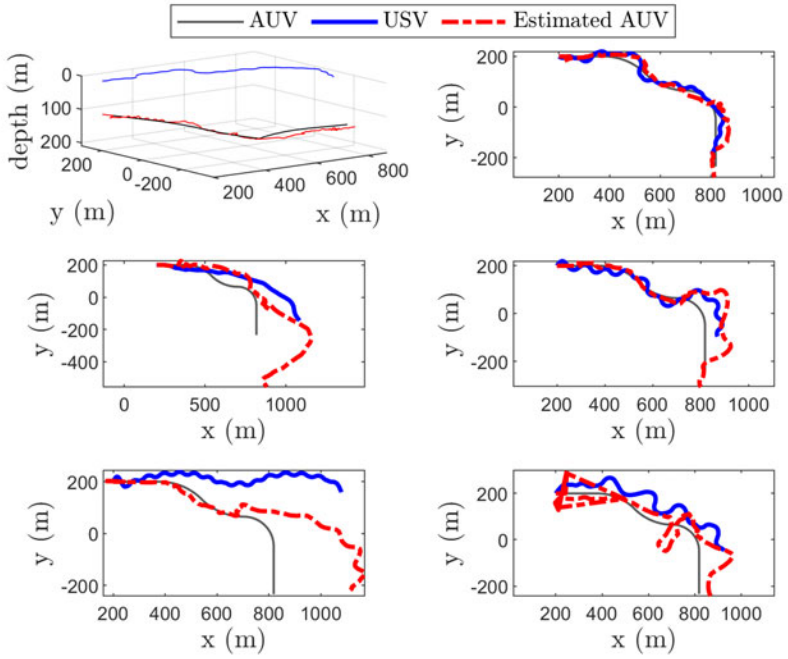

Fig. S9 USV moves along the optimized trajectory and the four specific trajectories in Case 5

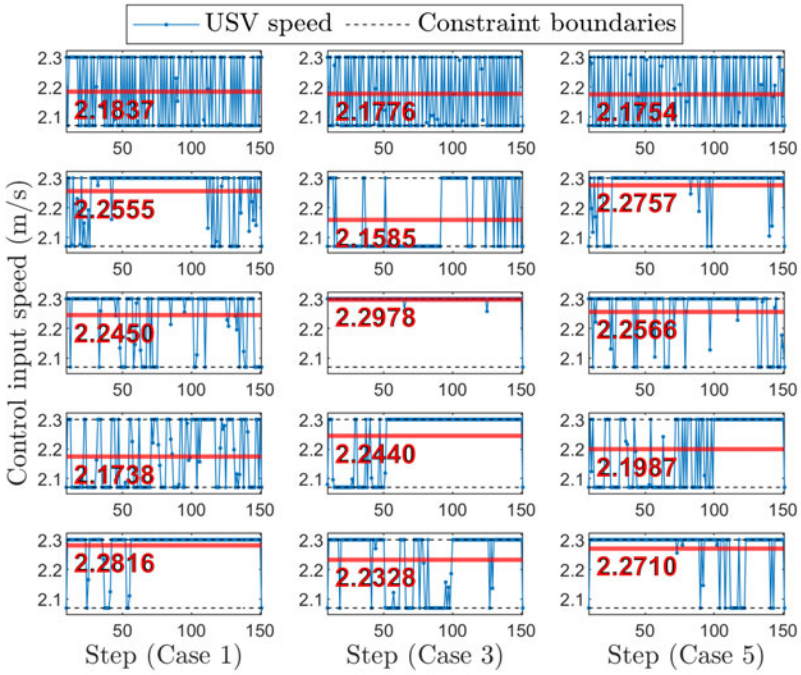

Fig. S10 USV speed control inputs. Columns represent Cases 1, 3, and 5, while rows correspond to the optimized, LinearFollow, SinFollow 1, SinFollow 2, and SinFollow 3 USV trajectories, respectively. The red line and the number below it indicate the MAS

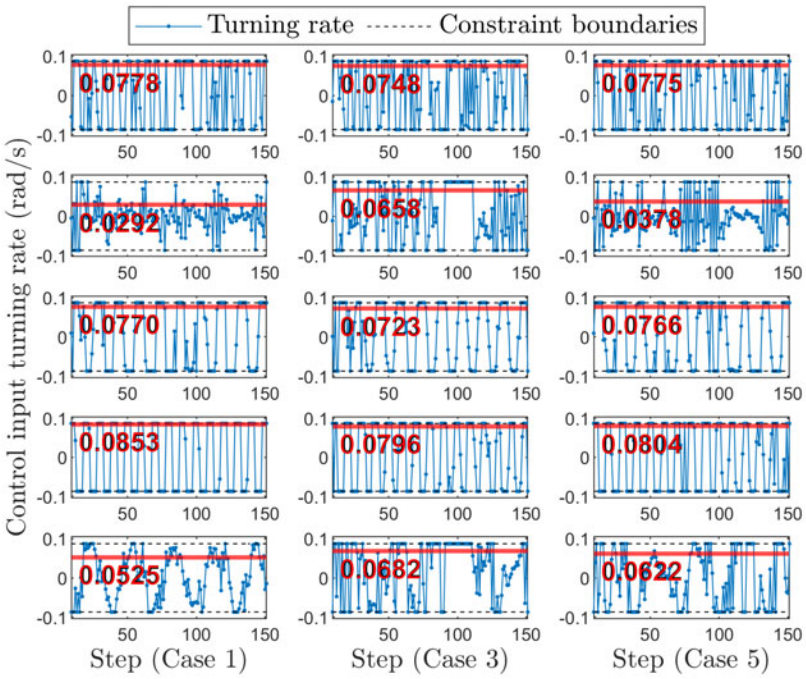

Fig. S11 USV turning rate control inputs. The red line and the number below it indicate the MATR